ROYAL SOCIETY OF CHEMISTRY

COMMUNICATION

Check for updates

Effects of annealing conditions on the battery anode properties of multilayer graphene due to layer exchange

R. Ito,[a] K. Nozawa,[a] N. Saitoh,[b] N. Yoshizawa,[c] T. Suemasu[a] and K. Toko [ID] *[a]

The annealing conditions of the layer-exchange synthesis of multi-layer graphene significantly affected its crystallinity and lithium-ion battery anode properties. We demonstrated excellent capacity retention and fast charge–discharge properties in multilayer graphene synthesized at low temperatures (400 °C). These results could contribute to the realization of flexible thin-film batteries.

Thin-film batteries with solid electrolytes have attracted considerable attention as a next-generation energy solution owing to their superior energy efficiency, cost-effectiveness, safety, and installation flexibility.[1,2] Graphite, which is commonly used as an anode material in conventional liquid lithium-ion batteries (LIBs), exhibits stable properties even when paired with other carrier ions[3,4] or solid electrolytes.[5] The synthesis of graphite as a thin film on various substrates could provide a reliable anode for advanced thin-film batteries. However, the synthesis of bulk graphite on any substrate is challenging as the synthesis temperature is usually above 1000 °C. Graphene, a two-dimensional sheet of graphite, has been synthesized at low temperatures using metal-catalyzed vapor-phase growth[6–10] or solid-phase growth.[11–13] As an anode material, graphene has an extremely high specific capacity because of its high specific surface area.[14–16] A stable operation over graphite has also been observed with multilayer graphene (MLG).[17–21] However, the use of a thin MLG anode is impractical because of its limited capacity per area. Obtaining thick MLG (*i.e.*, graphite thin film) through conventional low-temperature synthesis methods which involve heating the solid solution and cooling to precipitate carbon on metal catalysts remains challenging.

Layer exchange (LE) is a technique for forming polycrystalline semiconductor thin films on various substrates by exchanging layers of metal and amorphous semiconductors during a heat treatment process.[22–25] We discovered that eight different metals can induce LE with amorphous carbon (a-C), leading to the formation of MLG.[26–28] The resulting MLG exhibited properties comparable to those of bulk graphite when used as an anode electrode for LIBs.[29–31] The shape of the MLG conformed to that of the initial metal layer, allowing precise control of thickness control over a wide range.[32,33] In this study, we investigated the effect of LE synthesis temperature on the anode properties of MLG. Lower synthesis temperatures resulted in better anode properties, and paved the way for the development of flexible thin-film batteries using plastic substrates.

Fig. 1(a) illustrates the schematic of the LE process. We formed MLG using a Ni-induced LE with an inverted structure,
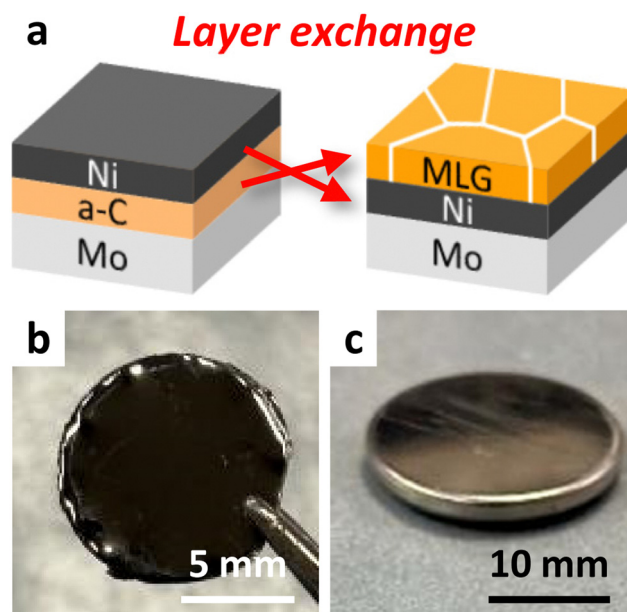

Fig. 1 Sample outline of this study. (a) Schematic of the LE process. Photographs of the (b) sample after LE and (c) coin cell battery.

[a] *Institute of Applied Physics, University of Tsukuba, 1-1-1 Tennodai, Tsukuba, Ibaraki 305-8573, Japan*

[b] *Electron Microscope Facility, AIST, 1-1-1 Higashi, Tsukuba, Ibaraki 305-8564, Japan*

[c] *Global Zero Emission Research Center, AIST, 16-1 Onogawa, Tsukuba, Ibaraki 305-8569, Japan*

which self-assembles into a Ni bottom electrode.[24,29] We sequentially deposited Ni and a-C thin films, each with a thickness of 200 nm, on Mo foils. All depositions were performed using radio-frequency (RF) magnetron sputtering (Sanyu Electron SVC-700RF, base pressure: 3.0×10^{-4} Pa) with Ar plasma. The RF power was set to 50 and 100 W for Ni and a-C, respectively. The samples were subjected to heat treatment at growth temperatures (T_g) of 800 °C for 10 min, 600 °C for 8 h, and 400 °C for 15 h. For $T_g = 600$ °C and 800 °C, the samples were removed from the sputtering equipment and annealed in a furnace (Koyo Thermo Systems KTF035N1) with an Ar atmosphere. For $T_g = 400$ °C, the sample was annealed inside the sputtering equipment without exposure to the atmosphere, a method that prevents oxygen contamination of the a-C films and enables crystallization at low temperatures.[24,34] We note that 400 °C was approximately the lower limit of annealing temperature at which layer exchange of carbon occurred, while carbon on the Mo substrate sublimated during annealing at 900 °C. Therefore, T_g ranged from 400 to 800 °C. The samples, as depicted in Fig. 1(b), were analyzed using Raman spectroscopy (JASCO NRS-5100; spot diameter, 5 μm; wavelength, 532 nm), scanning electron microscopy (SEM, Hitachi High-Technologies SU-8020), and transmission electron microscopy (TEM, FEI Tecnai Osiris) at 200 kV, equipped with energy dispersive X-ray (EDX). As shown in Fig. 1(c), coin-type cells were fabricated using the MLG electrode, pure Li metal foil, and a separator (Celgard 2400) immersed in an electrolyte. The electrolyte used was lithium hexafluorophosphate (LiPF$_6$) (1 mol L^{-1}) in ethylene carbonate (EC)/diethyl carbonate (DEC) (1 : 1 volume ratio). The characteristics of the anode were examined using an electrochemical measuring instrument (Meiden Hokuto HJ1001SD8).

Fig. 2(a) shows that the Raman spectra of all samples have peaks at approximately 1350, 1580, and 2700 cm^{-1}, which correspond to the D, G, and G′ peaks in the graphitic structure, respectively.[35] These results indicate that LE occurred in all T_g samples and that MLG was synthesized. Fig. 2(b) demonstrates that the G/D ratio, which corresponds to the crystallinity of MLG, is higher at lower T_g. For the sample synthesized at $T_g = 400$ °C, the G/D ratio reached 13.7, which is higher than that of most low-temperature-synthesized MLGs.[36–40] This trend in the G/D ratio is reasonable, considering that, in general, grain size expansion and orientation increase with lower temperatures in the LE process.[23] Annealing in vacuum, avoiding atmospheric exposure, may also have been effective in improving MLG crystallinity. Fig. 2(c)–(e) show that the surface morphology of MLG varies with T_g. All samples exhibited common directional linear patterns originating from the polishing marks on the Mo foil. At $T_g = 400$ °C, voids were observed in the MLG, suggesting partially incomplete LE. At $T_g = 600$ °C, the MLG formed relatively uniformly. At $T_g = 800$ °C, the MLG was relatively rough, which could be attributed to Ni agglomeration during high-temperature annealing.

We investigated the detailed cross-sectional structure of the sample synthesized at $T_g = 400$ °C. Fig. 3(a) shows that the film formed on Mo exhibits a complex stacking structure, which
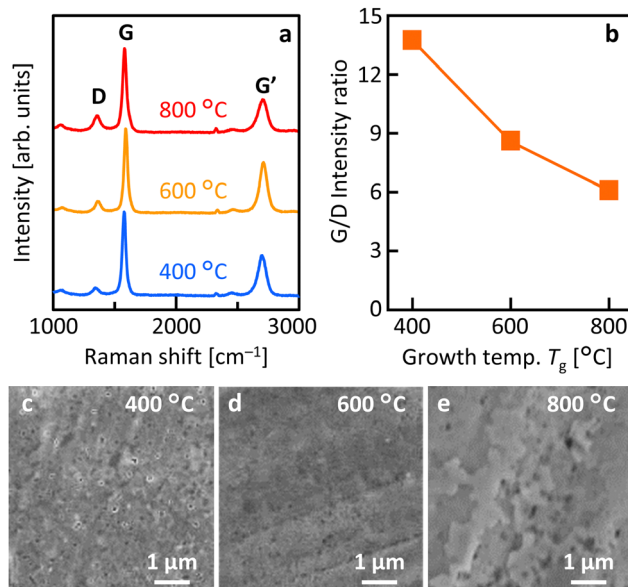

Fig. 2 T_g dependent growth morphologies. (a) Raman spectra obtained from the sample surface. (b) G/D intensity ratio of the samples determined by the Raman spectra shown in (a). SEM images of the samples for $T_g =$ (c) 400 °C, (d) 600 °C, and (e) 800 °C.
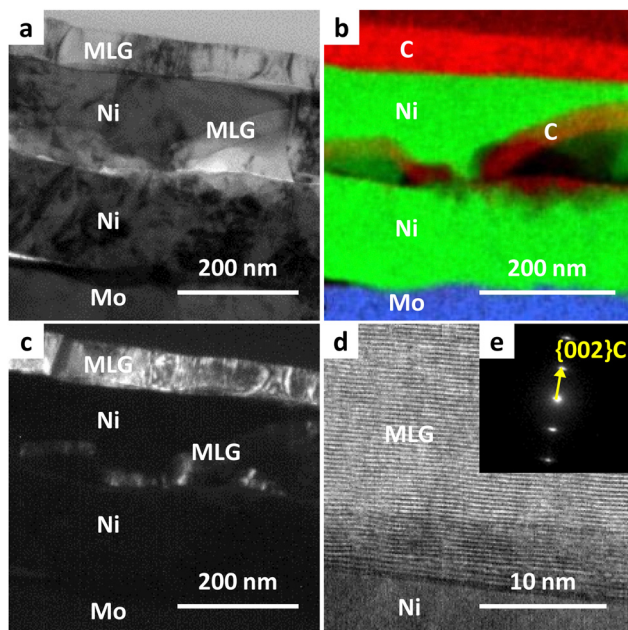

Fig. 3 Characterization of the cross-section of the sample for $T_g = 400$ °C. (a) Bright-field TEM image. (b) EDX elemental map. (c) Dark-field TEM image using the C{002} plane reflection. (d) High-resolution lattice images showing the lower part of the MLG layer. (e) Selected area electron diffraction pattern taken from the region including MLG with a selected area diameter of 200 nm.

differs from the structure typically obtained by standard inverted LE.[23,24] Fig. 3(b) indicates that MLG was formed on the top surface, with the Ni layer positioned at the bottom through the LE, while MLG was also present within the Ni layer.
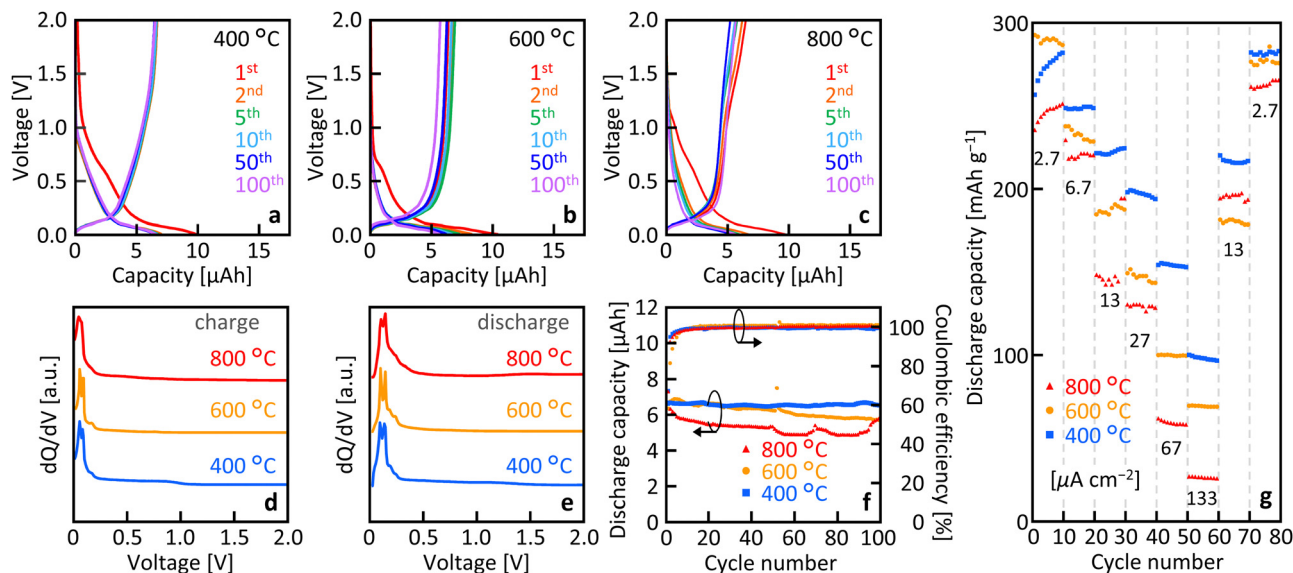
Fig. 4 Anode properties of the samples. Galvanostatic charge/discharge cycles of the samples for T_g = (a) 400 °C, (b) 600 °C, and (c) 800 °C, where the current density is 13 μA cm^{-2} dQ/dV plots of (d) charge and (e) discharge for the 10th cycle. (f) Discharge capacity and coulombic efficiency as a function of cycle number. (g) Current-rate testing of the samples at current densities ranged from 2.7 to 133 μA cm^{-2}, every 10 cycles.

A similar structure has been reported in the LE of the Si–Al system, which was attributed to nucleation occurring within the metal layer.[41,42] Fig. 3(c)–(e) illustrates that the MLG layers are oriented parallel to the Ni interface, a common characteristic of MLGs with high interfacial energy anisotropy. Notably, the lattice image in Fig. 3(d) suggests that the MLG is highly crystalline despite its low synthesis temperature.

Fig. 4(a)–(c) show that, for all T_g, the samples exhibited clear charge/discharge operation over 100 cycles. The initial charge capacity was elevated owing to the formation of a solid electrolyte interface (SEI) at 0.73 V, which resulted in a faradaic reduction of the electrolyte.[43] The quality of SEI would be roughly equivalent to bulk graphite, while there may be some heterogeneity due to the defects in the current MLG. Fig. 4(d) and (e) show a distinct peak around 0.06 V in the dQ/dV curve, which is a typical potential corresponding to the deinsertion of lithium ions into graphite.[21,44] Fig. 4(f) illustrates the cycle characteristics derived from the charge–discharge characteristics. For all samples, the coulombic efficiency was relatively low in the first cycle owing to irreversible capacity formation but maintained a high value of nearly 100% during subsequent cycles. As the number of cycles increased, the discharge

capacity gradually decreased for T_g = 600 °C and 800 °C, whereas it remained almost constant for T_g = 400 °C. The discharge capacity at T_g = 400 °C was 6.53 μAh after 100 cycles, which corresponds to about 98% of the initial cycle discharge capacity. Fig. 4(g) shows the current rate characteristics of the discharge capacity. Similar to general anodes, the capacitance decreases with increasing current rate, which is dependent on T_g. The capacitance tended to be higher at lower T_g values, particularly at higher current rates.

We observed the state of the MLG layers after disassembling coin cells that had undergone 100 charge/discharge cycles. Fig. 5 shows that the surface morphology depends on T_g. For the T_g = 400 °C sample, the MLG layer shows a uniform surface texture (Fig. 5(a)), which is the same as that before charge/discharge operation. In contrast, the T_g = 600 °C and 800 °C samples show cracks and partial delamination of the MLG layer, respectively (Fig. 5(b) and (c)). These behaviors indicate that the MLG layer was damaged during the charge/discharge process, likely due to the volume change caused by the deinsertion of lithium ions. These results agree with the T_g dependent charge/discharge characteristics. Based on the Raman results, it appears that the high crystallinity of the MLG synthesized at low temperatures may be responsible for its excellent film strength.
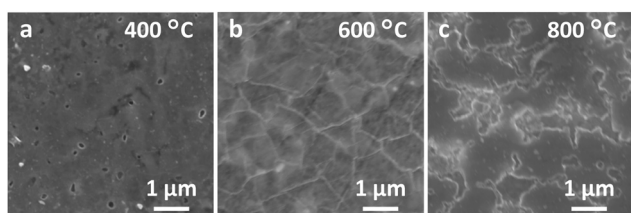
Conclusions

The effect of annealing conditions of MLG anodes on the LIB properties of MLG anodes was studied. The LE method allowed MLG to be synthesized within the temperature range of 400–800 °C. Raman measurements, electron microscopy, and charge–discharge analyses indicated that T_g affected the crystallinity and anode properties of MLG; a lower T_g resulted in

Fig. 5 Surface SEM images of the samples after 100 cycles of charge/discharge at the current density of 13 μA cm^{-2}, where T_g = (a) 400 °C, (b) 600 °C, and (c) 800 °C.

higher crystallinity and improved charge–discharge properties. Notably, the MLG synthesized at 400 °C exhibited excellent cycle stability and current rate performance, highlighting its potential for practical applications in flexible thin-film batteries. This study demonstrates that low-temperature synthesis of MLG is crucial for developing next-generation energy solutions.

Data availability

Data for this article are available at Open Science Framework at https://osf.io/tgrjs.

Conflicts of interest

There are no conflicts to declare.

Acknowledgements

Notes and references

1 H. Nishide and K. Oyaizu, Science, 2008, 319, 737–738.
2 Y. Pang, J. Pan, J. Yang, S. Zheng and C. Wang, Electrochem. Energy Rev., 2021, 4, 169–193.
3 M. Shen, H. Ding, L. Fan, A. M. Rao, J. Zhou and B. Lu, Adv. Funct. Mater., 2023, 33, 2213362.
4 P. Luo, P. Liu, W. Luo, H. Fu, J. Chen, H. Ding, C. Gao and B. Lu, J. Mater. Chem. A, 2024, 12, 16410–16418.
5 K. Takada, Acta Mater., 2013, 61, 759–770.
6 M. H. Rümmeli, A. Bachmatiuk, A. Scott, F. Börrnert, J. H. Warner, V. Hoffman, J.-H. Lin, G. Cuniberti and B. Büchner, ACS Nano, 2010, 4, 4206–4210.
7 J.-I. Fujita, T. Hiyama, A. Hirukawa, T. Kondo, J. Nakamura, S. Ito, R. Araki, Y. Ito, M. Takeguchi and W. W. Pai, Sci. Rep., 2017, 7, 12371.
8 H. J. Park, B. W. Ahn, T. Y. Kim, J. W. Lee, Y. H. Jung, Y. S. Choi, Y. I. Song and S. J. Suh, Thin Solid Films, 2015, 587, 8.
9 K. Murakami, S. Tanaka, A. Hirukawa, T. Hiyama, T. Kuwajima, E. Kano, M. Takeguchi and J. Fujita, Appl. Phys. Lett., 2015, 106, 093112.
10 Y. Nakajima, H. Murata, N. Saitoh, N. Yoshizawa, T. Suemasu and K. Toko, ACS Omega, 2019, 4, 6677–6680.
11 K. Koshida, K. Gumi, Y. Ohno, K. Maehashi, K. Inoue and K. Matsumoto, Appl. Phys. Express, 2013, 6, 105101.
12 J. Kwak, J. H. Chu, J.-K. Choi, S.-D. Park, H. Go, S. Y. Kim, K. Park, S.-D. Kim, Y.-W. Kim, E. Yoon, S. Kodambaka and S.-Y. Kwon, Nat. Commun., 2012, 3, 645.
13 Y. Chen, J. Wang, P. Schützendübe, Z. Wang and E. J. Mittemeijer, Carbon, 2020, 159, 37–44.
14 N. Li, Z. Chen, W. Ren, F. Li and H.-M. Cheng, Proc. Natl. Acad. Sci. U. S. A., 2012, 109, 17360–17365.
15 D. Wei, S. Haque, P. Andrew, J. Kivioja, T. Ryhänen, A. Pesquera, A. Centeno, B. Alonso, A. Chuvilin and A. Zurutuza, J. Mater. Chem. A, 2013, 1, 3177.
16 N. J. Dudney, Mater. Sci. Eng. B, 2005, 116, 245–249.
17 G. Radhakrishnan, J. D. Cardema, P. M. Adams, H. I. Kim and B. Foran, J. Electrochem. Soc., 2012, 159, A752.
18 H. Sun, A. Varzi, V. Pellegrini, D. A. Dinh, R. Raccichini, A. E. Del Rio-Castillo, M. Prato, M. Colombo, R. Cingolani, B. Scrosati, S. Passerini and F. Bonaccorso, Solid State Commun., 2017, 251, 88–93.
19 R. Mo, D. Rooney, K. Sun and H. Y. Yang, Nat. Commun., 2017, 8, 13949.
20 T. M. Paronyan, A. K. Thapa, A. Sherehiy, J. B. Jasinski and J. S. D. Jangam, Sci. Rep., 2017, 7, 39944.
21 H. Song, R. Na, C. Hong, G. Zhang, X. Li, Y. Kang, Q. Zhang and H. Xie, Carbon, 2022, 188, 146–154.
22 Z. Wang, L. Gu, F. Phillipp, J. Y. Wang, L. P. H. Jeurgens and E. J. Mittemeijer, Adv. Mater., 2011, 23, 854.
23 K. Toko and T. Suemasu, J. Phys. D: Appl. Phys., 2020, 53, 373002.
24 K. Toko and H. Murata, Nanotechnology, 2021, 32, 472005.
25 K. Toko, S. Maeda, T. Ishiyama, K. Nozawa, M. Murata and T. Suemasu, Adv. Electron. Mater., 2024, 10, 2400130.
26 H. Murata, K. Toko, N. Saitoh, N. Yoshizawa and T. Suemasu, Appl. Phys. Lett., 2017, 110, 33108.
27 H. Murata, N. Saitoh, N. Yoshizawa, T. Suemasu and K. Toko, Appl. Phys. Lett., 2017, 111, 243104.
28 Y. Nakajima, H. Murata, Y. Kado, R. Matsumura, N. Fukata, T. Suemasu and K. Toko, Appl. Phys. Express, 2020, 13, 025501.
29 H. Murata, Y. Nakajima, Y. Kado, N. Saitoh, N. Yoshizawa, T. Suemasu and K. Toko, ACS Appl. Energy Mater., 2020, 3, 8410–8414.
30 Y. Nakajima, H. Murata, Y. Kado, R. Matsumura, N. Fukata, T. Suemasu and K. Toko, Appl. Phys. Express, 2020, 13, 025501.
31 T. Suzuki, H. Murata, Y. Kado, T. Ishiyama, N. Saitoh, N. Yoshizawa, T. Suemasu and K. Toko, ACS Appl. Mater. Interfaces, 2022, 14, 54670–54675.
32 H. Murata, Y. Nakajima, N. Saitoh, N. Yoshizawa, T. Suemasu and K. Toko, Sci. Rep., 2019, 9, 4068.
33 D. Janke, F. Munnik, J. Julin, R. Hübner, J. Grenzer, C. Wüstefeld, S. Gemming, D. Rafaja and M. Krause, Carbon, 2020, 159, 656–667.
34 H. Murata, K. Nozawa, N. Saitoh, N. Yoshizawa, T. Suemasu and K. Toko, Appl. Phys. Express, 2020, 13, 055502.
35 L. M. Malard, M. A. Pimenta, G. Dresselhaus and M. S. Dresselhaus, Phys. Rep., 2009, 473, 51.
36 S.-J. Byun, H. Lim, G.-Y. Shin, T.-H. Han, S. H. Oh, J.-H. Ahn, H. C. Choi and T.-W. Lee, J. Phys. Chem. Lett., 2011, 2, 493.
37 K. Gumi, Y. Ohno, K. Maehashi, K. Inoue and K. Matsumoto, Jpn. J. Appl. Phys., 2012, 51, 06FD12.
38 M. Sato, M. Takahashi, H. Nakano, Y. Takakuwa, M. Nihei, S. Sato and N. Yokoyama, Jpn. J. Appl. Phys., 2014, 53, 04EB05.

39 M. Kosaka, S. Takano, K. Hasegawa and S. Noda, *Carbon*, 2015, **82**, 254.

40 Q.-Q. Zhuo, Q. Wang, Y.-P. Zhang, D. Zhang, Q.-L. Li, C.-H. Gao, Y.-Q. Sun, L. Ding, Q.-J. Sun, S.-D. Wang, J. Zhong, X.-H. Sun and S.-T. Lee, *ACS Nano*, 2015, **9**, 594.

41 M. Takeuchi and M. Kondo, *Jpn. J. Appl. Phys.*, 2014, **53**, 050303.

42 A. O. Zamchiy, E. A. Baranov, E. A. Maximovskiy, V. A. Volodin, V. I. Vdovin, A. K. Gutakovskii and I. V. Korolkov, *Mater. Lett.*, 2020, **261**, 127086.

43 P. Novák, F. Joho, R. Imhof, J. C. Panitz and O. Haas, *J. Power Sources*, 1999, **81**, 212.

44 M. D. Levi and D. Aurbach, *J. Electroanal. Chem.*, 1997, **421**, 79.